01 Jul 1997

Small Angle Neutron Scattering from Nanodroplet Aerosols

Barbara Ellen Wyslouzil

Janice L. Cheung

Gerald Wilemski
Missouri University of Science and Technology, wilemski@mst.edu

Reinhard Strey

Small Angle Neutron Scattering from Nanodroplet Aerosols

B. E. Wyslouzil,[1] J. L. Cheung,[1] G. Wilemski,[2,*] and R. Strey[3]
[1]*Department of Chemical Engineering, Worcester Polytechnic Institute, Worcester, Massachusetts 01609*
[2]*Lawrence Livermore National Laboratory, Livermore, California 94551*
[3]*Institut für Physikalische Chemie, Universität zu Köln, D-50939 Köln, Germany*
(Received 22 April 1997)

We report the first measurements of small angle neutron scattering from an aerosol. The aerosol was produced by expanding a D_2O-N_2 vapor mixture in a supersonic Laval nozzle. The neutron wavelength (0.5 nm) is less than the typical particle size, and we can therefore derive the average particle size (5–8 nm), number density ($\sim 10^{12}$ cm^{-3}), and polydispersity of the size distribution directly from the experimental data rather than by inferring them from complex models of particle formation and growth. We also predict and observe a Doppler shift-induced anisotropy in the scattering pattern due to the directed motion of the aerosol in the nozzle. Further applications of this new technique are discussed. [S0031-9007(97)03588-6]

PACS numbers: 61.12.Ex, 47.40.Ki, 64.70.Fx, 82.70.Rr

Small angle neutron scattering (SANS) is a powerful tool for examining the structure of matter in the 1–100 nm range. It has been used with great success to elucidate the properties of complex fluids such as microemulsions [1] and polymer solutions [2]. To our knowledge, it has never before been used to examine the properties of an aerosol, that is, a suspension of liquid droplets or solid particles in a carrier gas. The technical challenges that make this application so difficult are best understood by directly comparing the characteristics of aerosols and microemulsions. Microemulsions are relatively easy to examine using SANS because less than 1 cm^3 of material is required per sample, the samples are stable, the volume fraction of the disperse phase ν is usually in the range 0.01–0.9, and the droplet number density N is typically $>10^{16}$ cm^{-3}. An aerosol, in contrast, is not stable and must be produced continuously in the neutron beam line. Furthermore, the scattering signals from aerosols will be many orders of magnitude smaller than from microemulsions because ν generally lies below $\sim 10^{-5}$, and finite nucleation rates and rapid coagulation combine to keep N below $\sim 10^{14}$ cm^{-3}.

Despite these technical difficulties, there are compelling reasons for applying SANS to an aerosol of nanoparticles. First, particles with radii $r < 10$ nm are of special interest because they lie at the transition between large molecular clusters and the bulk. Second, examining an aerosol *in situ* with a noninvasive technique can deepen our fundamental understanding of aerosol formation and growth processes. An even more exciting prospect is our eventual goal of using SANS to determine the composition and internal structure of multicomponent nanometer sized droplets. Before tackling these more exotic applications, however, we must first prove that aerosol SANS experiments are feasible.

Below we describe the first successful application of SANS to study a condensation aerosol. We used D_2O for these experiments because of its similarity to H_2O, an important subject of condensation studies, and because its large scattering length and low incoherent scattering cross section enhance the coherent scattering signal. To reliably produce aerosols with $N \simeq 10^{12}$ cm^{-3} and a mean particle radius $\langle r \rangle < 10$ nm [3], we used a supersonic nozzle to rapidly expand dilute vapor mixtures of D_2O and N_2.

The basic features of condensation in a supersonic nozzle are well understood [4,5]. In the absence of condensation, the pressure, density, and temperature of the gas mixture fall isentropically as the expansion proceeds (see Fig. 1). The rapid temperature decrease causes the condensable vapor to become highly supersaturated, and the rate of particle formation by homogeneous nucleation increases rapidly. Peak nucleation rates (inferred by

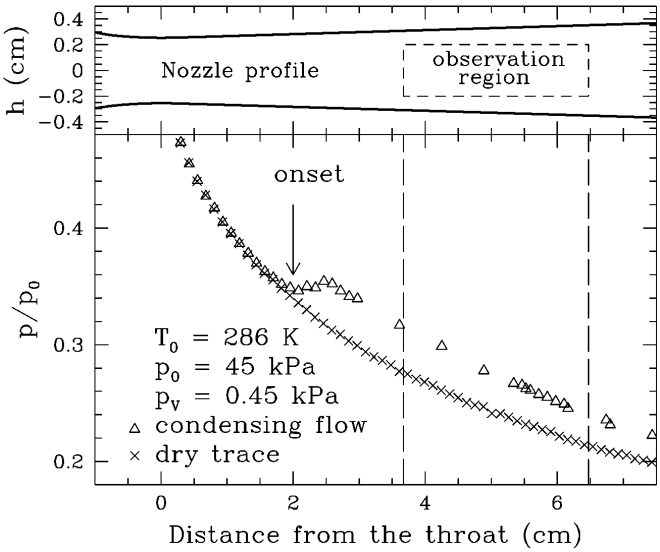

FIG. 1. Top: a longitudinal section through the nozzle shows the location of the observation region. The nozzle has a rectangular cross section; the throat height and width are 0.5 and 1.23 cm, respectively. Downstream of the throat the upper and lower nozzle walls diverge at an angle of 1.8°. Bottom: pressure traces for conditions close to those of experiment 3.

modeling [4]) can easily reach $10^{18}\ \mathrm{cm}^{-3}\,\mathrm{s}^{-1}$. Growth of the particles depletes the vapor, quenching nucleation. Consequently, most of the particles form in a burst of nucleation lasting only a few microseconds. The phase transition is accompanied by latent heat release that renders condensation observable as a deviation of the pressure (or density) from the isentropic profile (see Fig. 1). The total heat released per unit volume of flow, Q ($\propto N\langle r^3\rangle$), can be determined from the measured isentropic and condensing flow curves [4,5]. Unfortunately, it is not possible to uniquely determine N, $\langle r\rangle$, and the width of the aerosol size distribution, σ, from this information [6].

Light scattering can complement pressure or density measurements [6], but its utility is limited because the droplets ($\sim$1–10 nm) are much smaller than the wavelength of visible light ($\lambda \sim 400$–700 nm). In the Rayleigh regime, ($\langle r\rangle/\lambda \ll 1$), the light scattering intensity is proportional to $N\langle r^6\rangle$ and is independent of the observation angle. To determine N and $\langle r\rangle$ from $N\langle r^3\rangle$ and $N\langle r^6\rangle$ requires the strong and generally invalid assumption that the aerosol is monodisperse.

The advantage of cold neutrons over light for probing nanoparticle aerosols is that the wavelength range, $\lambda \simeq 0.5$–2 nm, is comparable to $\langle r\rangle \simeq 1$–$10$ nm. Because the neutron scattering intensity $I(q)$ is a strong function of the momentum transfer wave vector, q, in the experimentally accessible range, we can obtain reliable values for N, $\langle r\rangle$, and σ directly from the data with only a much weaker assumption about the general shape of the size distribution, e.g., Gaussian or log normal.

Our Laval nozzle, depicted in Figs. 1 and 2, is machined from aluminum following the simple design described by Stein [7]. The side walls contain $2.5 \times 7.5\ \mathrm{cm}^2$ Si windows that are 1 mm thick and are essentially transparent to the neutrons. An advantage of this type of Laval nozzle is that the droplet number density and velocity along the optical path are constant because the flow is one dimensional and the droplets move at right angles to the neutron beam in the geometry of our experiment.

Maintaining steady supersonic flow requires a large, constant N_2 flow rate, e.g., 0.25 mol/s at a plenum pressure of 44 kPa. To achieve this, we vaporize liquid N_2 in an aluminum heat exchanger consisting of six 3 m long finned tubes using room air as the heat source. At steady state, the N_2 exits the heat exchanger slightly below room temperature, and D_2O is added to the gas stream by evaporation from a heated piece of felt fed by a syringe pump. After the vapor mixture is cooled to the desired temperature, a high accuracy humidity probe (HMP233, Vaisala Inc.) measures the vapor phase activity of D_2O [8]. The mixture then enters the plenum, where the temperature and pressure of the gas "at rest" are measured. After traversing a short flow straightener, the gas moves into the nozzle. The flow through the system is maintained by two Busch rotary vane vacuum pumpsthat have a combined capacity of 0.13 m^3/s. The entire apparatus is portable.

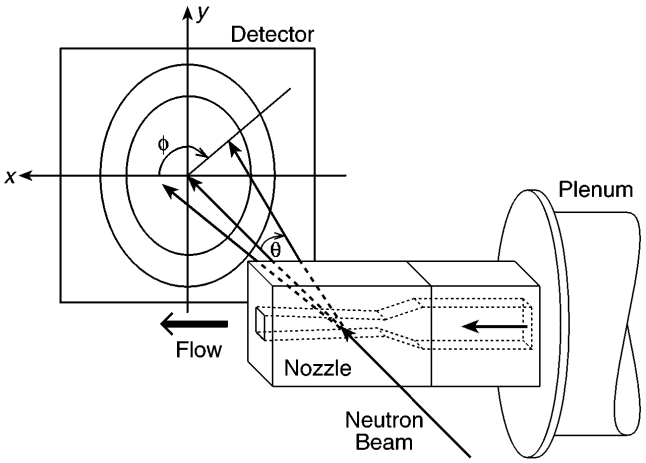

FIG. 2. The aerosol is formed in the nozzle which sits in the neutron beam. The scattering angles θ and ϕ are defined. Two contour lines of constant scattering intensity are shown on the detector.

We used the NG7 beam line at NIST in Gaithersburg with the detector placed 7.3 m from the nozzle at a 0.2 m offset corresponding to a q range of $0.1 \le q \le 3\ \mathrm{nm}^{-1}$. To enhance signal intensity we used a long scattering zone, shown in Fig. 1, well downstream of onset, where the particle size distribution changes very slowly because condensation is nearly complete. The raw scattering intensity was corrected by subtracting the scattering intensity of the nozzle in the absence of condensation. The corrected scattering intensity was then normalized by dividing by the incoherent scattering intensity of H_2O and placed on an absolute scale by calibrating with a standard silica gel cell. We used 0.5 nm wavelength ($\Delta\lambda/\lambda = 0.15$) neutrons because the neutron flux is highest at short wavelengths. We examined five different condensable vapor concentrations, and for one condensable partial pressure, $p_v = 1.07$ kPa, we varied the total plenum pressure. Table I summarizes the experimental conditions and results.

An interesting complication in our experiments, arising from the directed motion of the particles, is that the momentum of the scattered neutrons is Doppler shifted in the laboratory reference frame. By analyzing the kinematics of two body elastic scattering, we may express q in terms of the laboratory variables as [10]

$$q = q_i\left[1 + \frac{v_p}{v_n}\sin\theta\cos\phi + \left(\frac{v_p}{v_n}\cos\phi\right)^2\right]^{1/2}. \quad (1)$$

Here, $q_i = (4\pi/\lambda_i)\sin(\theta/2)$, λ_i is the wavelength of the incident neutrons, v_p is the particle velocity, v_n is the incident neutron velocity, θ is the usual laboratory scattering angle, and ϕ is the azimuthal angle in the plane of the detector (see Fig. 2). Since the velocity of the particles in the observation region is $\sim$400 m/s or roughly 50% of the speed of the 800 m/s neutrons, q may differ from q_i by up to 14%. For slower neutrons, the differences increase. The resulting 2D scattering intensity

TABLE I. Summary of the experimental conditions and results. Shown are the total pressure p_0, condensable vapor pressure p_v, inlet temperature T_0 in the plenum (nozzle inlet), our best modeling estimates for the temperature T and particle velocity v_p in the observation region [9], the Guinier slope and intercept, and $\langle r\rangle$, σ, and N. We estimate that the latter three values are accurate to $\pm 20\%$.

Expt. No.	p_0 (kPa)	p_v (D_2O) (kPa)	T_0 (K)	T (K)	v_p (m/s)	Slope (nm^2)	Intercept $\ln[I(0)]$	$\langle r\rangle$ (nm)	σ (nm)	N (10^{12} cm^{-3})
7	58 ± 1.3	1.30 ± 0.05	304 ± 0.4	241–253	410–450	−27.45	−2.834	7.8	2.3	1.4
6	67 ± 4.0	1.07 ± 0.04	299 ± 0.4	227–242	410–460	−25.96	−3.170	7.1	2.4	1.4
5	60 ± 1.3	1.07 ± 0.04	299 ± 0.4	231–244	410–450	−26.47	−2.979	7.5	2.3	1.4
4	44 ± 1.3	1.07 ± 0.04	299 ± 0.4	240–251	400–440	−24.80	−3.156	7.1	2.3	1.5
1	44 ± 1.3	0.80 ± 0.03	293 ± 0.4	226–239	410–450	−20.22	−3.712	6.3	2.1	1.7
2	44 ± 1.3	0.60 ± 0.01	289 ± 0.4	217–231	400–440	−17.70	−4.078	5.6	2.1	2.0
3	44 ± 1.3	0.47 ± 0.01	286 ± 0.4	210–224	400–440	−14.22	−4.635	5.2	1.8	2.0

pattern is anisotropic in the laboratory reference frame and may be calculated from [10]

$$I(q) = \Sigma_j N(r_j) P(q, r_j) \left(1 + 2\frac{v_p}{v_n} \sin\theta \cos\phi\right), \quad (2)$$

where $N(r_j)$ is the number density of particles with radius r_j, $P(q, r_j)$ is the particle form factor [11], and q is defined in Eq. (1). The droplet motion changes the usual circular scattering pattern into a nearly elliptical one (see Fig. 2). Figure 3 shows experimental and theoretical traces of scattering intensity as a function of ϕ at constant θ. The predictions were made with Eqs. (1) and (2) and the experimental Gaussian particle distribution for spherical droplets (see below and Table I). The good agreement supports the theory. Properly interpreted, better data of this type will enable us to directly determine particle velocities.

Figure 4 shows $\bar{I}(q_i)$, the absolute scattering intensity averaged over ϕ versus q_i for experiment 1 after almost 5 h of signal integration. For experiments 2–7, we integrated for shorter times, 7 min–2 h, to minimize D_2O consumption and to maximize the number of conditions we could observe. All of the scattering patterns are similar to the pattern shown in Fig. 4 and are consistent with those for a unimodal, polydisperse distribution of spherical droplets.

To extract the key parameters of the particle size distributions, we first made a Guinier plot for each data set (see Fig. 5) and fit the linear region (9.8×10^{-3} $nm^{-2} < q_i^2 < 1.2 \times 10^{-1}$ nm^{-2}) using a weighted least-squares procedure [12]. We then fit calculated scattering curves to the experimental results by varying $\xi(= \sigma/\langle r\rangle)$ [13]. The calculations were made with Eqs. (1) and (2), a Gaussian form for $N(r_j)$, $v_p = 400$ m/s, and the scattering length density, $\rho_{D_2O} = 6.4 \times 10^{10}$ cm^{-2} [14].

From Table I, we see that $\langle r\rangle$ increases with p_v but does not depend strongly on p_0 and that σ increases with p_v while N decreases. These trends are consistent with our understanding of nucleation and growth in a supersonic nozzle since a higher value of p_v leads to particle formation over a longer time period and thus to a broader size distribution [6]. Values of ν derived from the SANS data are also consistent with the initial vapor concentrations.

In conclusion, our experiments clearly demonstrate that SANS can be successfully used to study the properties of nanodroplet aerosols. The angularly resolved, absolute

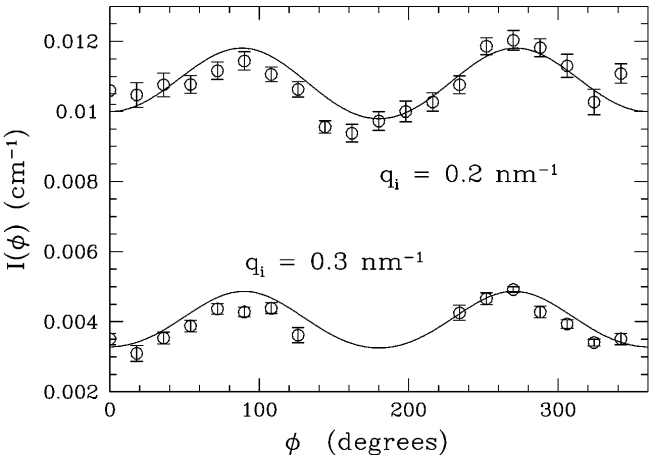

FIG. 3. The ϕ dependence of the scattering intensity at constant θ for experiment 1. Experimental and theoretical traces are shown for θ corresponding to $q_i = 0.2$ and 0.3 nm^{-1}.

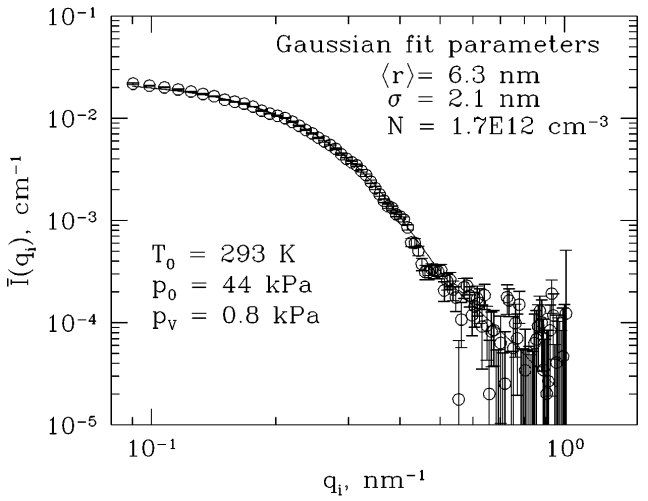

FIG. 4. The SANS spectrum for D_2O nanodroplets in the supersonic nozzle for experiment 1. The solid line is calculated for a droplet distribution with the parameters shown.

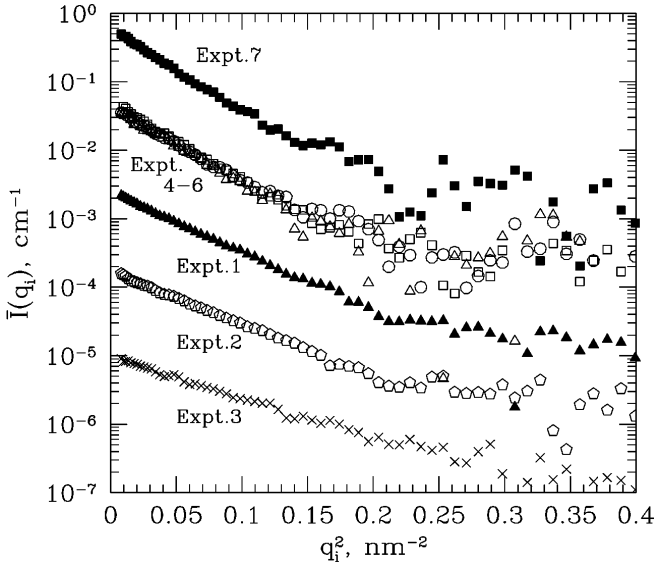

FIG. 5. The Guinier plots for the seven data sets. The intensities for experiments 4, 5, and 6 are on an absolute scale. For clarity, the other data sets have been offset by factors of 10, and error bars have been omitted. The good agreement among experiments 4–6 shows that any p_0 dependence is smaller than our current experimental uncertainty range.

scale intensity measurements let us draw a far more detailed picture of the aerosol than was previously possible using conventional light scattering. Even with these preliminary experiments, we were able to confirm the spherical nature of the droplets and, moreover, determine their concentration, mean radius, and polydispersity. In future experiments we will reduce the background scattering so the inflection seen in the theoretical curve in Fig. 4 at higher q should be clearly observed. With cleaner data, direct Fourier transformation [15] should then permit us to extract the interfacial profile. Furthermore, it should be possible to experimentally determine the composition of uniformly mixed binary droplets. Finally, the study of multicomponent droplets with inhomogeneous distributions of matter will become accessible to direct experimental determination.

We thank Mr. J. Winkler and our local NIST contacts, Dr. J. Barker and Dr. C. Glinka for their help. The National Institute of Standards and Technology, U.S. Department of Commerce, provided the neutron research facilities used in this work. This work was supported by NSF Grants No. CHE-9502604 and No. CHE-9522127, by the Petroleum Research Fund of the ACS, by NATO Travel Grant No. CRG-950768, and by the U.S. DOE, OBES, Division of Geosciences and Engineering. Part of this work was performed under the auspices of the U.S. Department of Energy by the Lawrence Livermore National Laboratory under Contract No. W-7405-ENG-48.

*New address: Physics Dept., Univ. Missouri, Rolla, MO 65409

[1] M. Kotlarchyk, S. H. Chen, J. S. Huang, and M. V. Kim, Phys. Rev. A **29**, 2054 (1984); E. Caponetti, L. J. Magid, J. B. Hayter, and J. S. Johnson, Jr., Langmuir **2**, 722 (1986); M. Gradzielski, D. Langevin, L. Magid, and R. Strey, J. Phys. Chem. **99**, 13 232 (1995).

[2] K. Mortensen, J. Phys. Condens. Matter **8**, A103 (1996).

[3] Angle brackets $\langle \cdots \rangle$ denote number averages over the aerosol particle size distribution.

[4] P. P. Wegener and B. J. C. Wu, Adv. Colloid Interface Sci. **7**, 325 (1977).

[5] B. E. Wyslouzil, G. Wilemski, M. G. Beals, and M. Frish, Phys. Fluids **6**, 2845 (1994).

[6] C. A. Moses and G. D. Stein, J. Fluids Eng. **100**, 311 (1978).

[7] G. D. Stein, Ph.D. thesis, Yale University, 1967 (unpublished).

[8] We calibrated the humidity probe against known D_2O partial pressures, confirmed that the readings are not a function of the carrier gas pressure, and showed that the humidity readings are not a function of the gas velocity.

[9] Here, v_p equals v, the local gas stream velocity. There is no slip between the gas stream and such small particles. Although here T and v are adequately found from gasdynamic modeling, they can both be directly determined by analyzing measured pressure traces for flows with condensation [4,5].

[10] G. Wilemski (unpublished). The equation shown holds for $v_p/v_n < 0.7$, small θ values, and massive particles.

[11] *Small Angle X-ray Scattering*, edited by O. Glatter and O. Kratky (Academic, London, 1982).

[12] By analyzing synthetic scattering curves for Gaussian particle distributions $(\propto (2\pi\sigma^2)^{-1/2} \exp[-(r_j - \langle r \rangle)^2/(2\sigma^2)])$ of different σ, we found that for the typical range, $0.1 < \sigma/\langle r \rangle < 0.5$, the Guinier relationship remains valid at much larger values of qr than for a monodisperse aerosol.

[13] When $\ln \bar{I}(q_i)$ is plotted versus q_i^2, the Guinier slope equals $r_G^2[1 + \frac{1}{2}(v_p/v_n)^2]/3$. For a polydisperse droplet distribution, the effective radius of gyration is $r_G^2 = \frac{3}{5}\langle r^8 \rangle/\langle r^6 \rangle$. For a Gaussian distribution centered on $\langle r \rangle$, with $\xi \leq 1/2$, the moments are accurately approximated by $\langle r^n \rangle = \langle r \rangle^n n! \sum_k' \xi^k/[2^{k/2}(k/2)!\,(n-k)!]$; the primed sum indicates that only even values of k, $0 \leq k \leq n$, are summed over. With the experimental Guinier slopes and intercepts and the above relationships, it is straightforward to vary ξ and minimize the sum of the weighted, squared residuals for the predicted and experimental values of $\ln[\bar{I}(q_i)/I(0)]$. Once the best value of ξ has been determined, $\langle r \rangle$ is found from r_G^2, N is calculated from $I(0) = 16\pi^2 \rho_{D_2O}^2 N \langle r^6 \rangle/9$, and $\nu = 4\pi N \langle r^3 \rangle/3$.

[14] This value is based on the density of $D_2O(l)$ at 298 K. The droplet temperature in the observation zone is about 240 K, but the density changes due to decreased temperature and increased pressure in the droplet cancel.

[15] O. Glatter, Prog. Colloid Polym. Sci. **84**, 46 (1991); R. Strey, O. Glatter, K.-V. Schubert, and E. W. Kaler, J. Chem. Phys. **105**, 1175 (1996).